Optoelectronic Inactivity of Dislocations in Cu(In,Ga)Se$_2$ Thin Films

Daniel Abou-Ras,* Aleksandra Nikolaeva, Maximilian Krause, Lars Korte, Helena Stange, Roland Mainz, Ekin Simsek Sanli, Peter A. van Aken, Takeyoshi Sugaya, and Jiro Nishinaga

High-efficiency Cu(In,Ga)Se$_2$ (CIGS) thin-film solar cells are based on poly-crystalline CIGS absorber layers, which contain grain boundaries, stacking faults, and dislocations. While planar defects in CIGS layers have been investigated extensively, little is still known about the impact of dislocations on optoelectronic properties of CIGS absorbers. Herein, evidence for an optoelectronic inactivity of dislocations in these thin films is given, in contrast to the situation at grain boundaries. This unique behavior is explained by the extensive elemental redistribution detected around dislocation cores, which is connected with the dislocation strain field, probably leading to a shift of defect states toward the band edges.

1. Introduction

Thin-film solar cells with record conversion efficiencies of more than 23%[1] are based on polycrystalline Cu(In,Ga)Se$_2$ (CIGS) absorbers. Planar defects such as stacking faults (including twin boundaries as special cases) and random grain boundaries in these absorbers have been studied to a large extent.[2] It was shown that also in highly efficient devices, enhanced

Dr. D. Abou-Ras, Dr. A. Nikolaeva, M. Krause, Dr. L. Korte, Dr. H. Stange, Dr. R. Mainz
Helmholtz-Zentrum Berlin für Materialien und Energie GmbH
Hahn-Meitner-Platz 1, Berlin 14109, Germany
E-mail: daniel.abou-ras@helmholtz-berlin.de

Dr. E. Simsek Sanli, Prof. P. A. van Aken
Stuttgart Center for Electron Microscopy
Max Planck Institute for Solid State Research
Heisenbergstr. 1, Stuttgart 70569, Germany

Dr. T. Sugaya, Dr. J. Nishinaga
Research Center for Photovoltaics
National Institute of Advanced Industrial Science and Technology (AIST)
Tsukuba, Baraki 305-8568, Japan

Dr. T. Sugaya, Dr. J. Nishinaga
Renewable Energy Research Center
National Institute of Advanced Industrial Science and Technology (AIST)
Koriyama, Fukushima 903-0298, Japan

The ORCID identification number(s) for the author(s) of this article can be found under https://doi.org/10.1002/pssr.202100042.

nonradiative recombination at grain boundaries leads to losses in open-circuit voltage of 20–30 mV.[3] In contrast, the optoelectronic properties of dislocations in CIGS thin films have not yet been assessed unambiguously.

Indeed, dislocations and partial dislocations in polycrystalline CIGS thin films were identified and characterized by means of transmission electron microscopy (TEM) in various CIGS thin films, in some cases at very high concentrations of 10^{10}–10^{11} cm^{-2}.[4,5] Still, in these CIGS thin films containing clearly visible dislocation clusters, enhanced recombination at these dislocations was not detectable, neither by electron-beam-induced current (EBIC) nor by cathodoluminescence (CL) analyses.[6] Nevertheless, a direct link between the presence of dislocations and their optoelectronic properties has so far not been provided.

This work fills this gap using epitaxial CIGS thin films as a model system, in which only dislocations and antiphase domain boundaries are present. It will be shown that CL images acquired at dislocations do not show any reduced signal as compared to the bulk material. Thus, these line defects seem optoelectronically inactive in CIGS thin films.

2. Experimental Details

Epitaxial CIGS layers were grown on p$^+$-type GaAs (001) substrates using molecular beam epitaxy. First, the GaAs substrates were etched in an alkaline etchant and loaded into the growth chamber. Native oxide layers on the GaAs surfaces were removed by a thermal flash anneal at 560 °C in an atomic hydrogen atmosphere. A 2.2 μm-thick CIGS layer was deposited by coevaporation of Cu, In, Ga, and Se at 520 °C. A uniform Na concentration of more than 2×10^{18} cm^{-3} was realized by NaF doping (confirmed by means of secondary-ion mass spectroscopy). The [Ga]/([Ga] + [In]) (GGI) ratio was controlled by adjusting the flux ratio of Ga and In. The GGI was fixed to be 0.6 to match the lattice constant of CIGS with that of GaAs. The [Cu]/([Ga] + [In]) (CGI) was controlled by adjusting the flux ratio of Cu and Ga/In. The CGI of the CIGS layers was set to 0.85 to suppress the formation of the Cu$_2$Se phase, and the CGI was confirmed by electron probe microanalysis. The beam-equivalent pressure of Se was fixed to about 3×10^{-3} Pa.

After CIGS deposition, KF postdeposition treatment in Se atmosphere was carried out at 350 °C for 10 min. Finally, a CdS layer from a chemical bath and an Al-doped ZnO layer by direct-current magnetron sputtering were deposited as buffer and window layers. Epitaxial CIGS layers have very flat surfaces and thus, i-ZnO layers are not needed to suppress low shunt resistivity. Therefore, we deposited Al-doped ZnO layers directly on a CdS buffer layer, and the solar cells exhibited low series resistivities.

Polycrystalline $CuInSe_2$ thin films were grown by a three-stage coevaporation process[7] on a 12 nm-thick NaF precursor layer on top of Mo-coated soda-lime glass. The growth process was intentionally interrupted during Cu–Se deposition at a point, where the [Cu]/[In] ratio was 0.92 by closing the shutter of the Cu source.[8] Scanning electron microscopy (SEM) images were acquired using a Zeiss UltraPlus scanning electron microscope operated at 15 kV and 5 nA using InLens and angle-selective backscatter electron detectors. The CL hyperspectral images were recorded using a Zeiss Merlin scanning electron microscope equipped with a DELMIC CL system at 10 keV beam energy and at a beam current of 1 nA.

For the scanning transmission electron microscopy (STEM) investigation, a thin lamella was prepared using a Zeiss Crossbeam XB 1540 EsB. The electron energy-loss spectrometry (EELS) measurements in STEM were carried out at 200 kV on a probe-corrected (DCOR, CEOS GmbH) JEOL ARM 200F microscope equipped with a cold field-emission gun and a Gatan GIF Quantum ERS spectrometer. The angular range of the high-angle annular dark-field (HAADF) detector was set to 109–270 mrad for imaging. The beam convergence semiangle was 28 mrad for imaging and the collection semiangle was 111 mrad for EELS investigations. EELS spectrum images were acquired in DualEELS mode at 1 eV/channel dispersion covering the core energy-loss range from 300 to 2348 eV. The linear image distortion was corrected by means of the STEM SI Warp software suite.[9]

3. Results

To investigate the optoelectronic properties of dislocations, we chose epitaxially grown CIGS thin films in completed solar-cell stacks as a model system (**Figure 1**a). These layers do not exhibit any grain boundaries, but only dislocations and antiphase boundaries. The conversion efficiencies of these solar cells were about 20%, i.e., the results shown in the following were obtained on high-efficiency devices. To detect the locations of dislocations, electron-channeling contrast imaging (ECCI)[10] in SEM was applied (Figure 1a). Indeed, in SEM images acquired on cross-section specimens of solar cells with a stacking sequence of ZnO:Al/CdS/CIGS/GaAs, dislocations as well as antiphase domain boundaries (APB) are visible clearly as white lines within the dark CIGS layer (Figure 1b).

CL hyperspectral images were acquired at room temperature on the identical positions as the SEM images (Figure 1c), with a CL intensity distribution extracted along the arrow (Figure 1d, average across 20 pixels). No contrast at the positions of the dislocations or at antiphase domain boundaries is visible (also confirmed by CL linescans

extracted across the dislocations, see Figure S1, Supporting Information). This is consistent with findings in literature: CL images acquired on various CIGS thin films do not exhibit any significant contrast within individual grains that could be related to the presence of dislocations.[11–14] In contrast, CL signals exhibit decreased intensities at the positions of (randomly oriented) grain boundaries in polycrystalline CIGS thin films, due to enhanced nonradiative recombination.[12–14] We note that the present results are astonishing as dislocations in various semiconductor materials have shown to produce strong contrasts in CL images.[15–19] However, the CL results in Figure 1 suggest that the recombination velocities for dislocations (and for the detected antiphase domain boundaries) in CIGS are negligible and that their recombination behavior is similar to that of the CIGS bulk. We can exclude that the detected, homogeneous CL intensity map is simply a result of superimposed CL signals from a large density of dislocations, as it is apparent from the SEM image that the dislocations are not homogeneously distributed, but rather imhomogeneously dispersed across the CIGS layer.

To judge whether SEM as well as CL hyperspectral imaging are appropriate techniques to study dislocations in CIGS thin films in terms of sufficient spatial resolutions, it is important to consider the information volumes from which electrons and luminescence are emitted and detected by the corresponding detectors, and not the excitation volume of electron–hole pairs at 10 keV and 1 nA. For SEM imaging, which uses a channeling contrast, it is known that dislocations can be resolved clearly (see the study by Zaefferer and Elhami[10]); thus, we can assume a spatial resolution on the order of few 10 nm. As for the corresponding value of the CL signals, they can be estimated to about 100 nm (order of magnitude), from various CL analyses on grain boundaries in polycrystalline CIGS layers,[3,12] in which the contrasts of grain boundaries were clearly detectable, in spite of at times small grain diameters of down to about 100 nm. Although the diffusion of excited charge carriers prior to the radiative recombination has to be considered, the recombination rates of excited electrons and holes are rather high due to probable high-injection conditions during the CL experiment at 10 keV and 1 nA. Thus, also the flux of the emitted luminescence is very large already right after the excitation of the charge carriers, prior to the effective diffusion, which is the reason for the high spatial resolution in CL images obtained on the CIGS layers. Altogether, the spatial resolutions of SEM and CL hyperspectral imaging are on the order of several 10 and 100 nm, which is appropriate to detect the positions and the optoelectronic properties of dislocations in CIGS layers.

4. Discussion

What can be the reason for this exceptional behavior of the dislocations in CIGS? When probing the elemental distributions at and around dislocation cores in polycrystalline $CuInSe_2$ thin films at the atomic scale, copious Cu redistribution was found for dislocation cores located at grain boundaries (yellow line in **Figure 2**a). In Figure 2b,c, it is apparent that Cu (In) is enriched (depleted) in the upper right corner, whereas Cu (In) is depleted
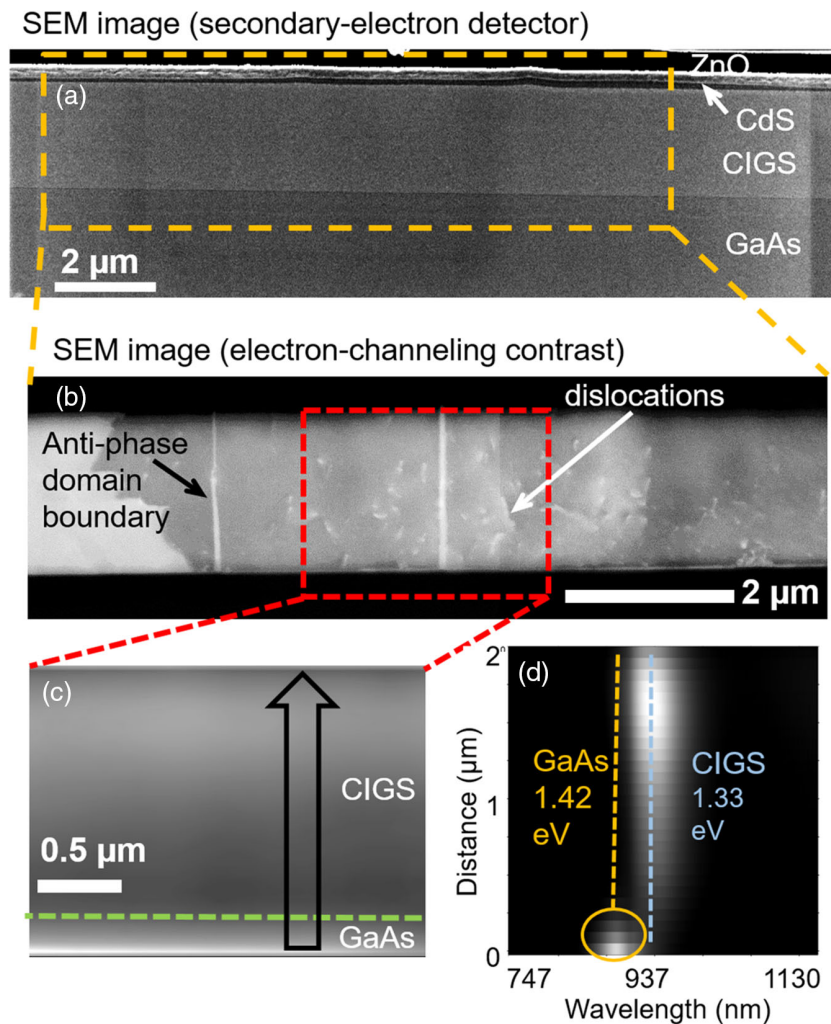
Figure 1. a,b) SEM images acquired on cross-section specimens from a ZnO:Al/CdS/CIGS/GaAs stack using an InLens secondary electron detector (a) and an angle-selective backscattered electron detector (b) c) CL intensity map recorded on the area highlighted by the red rectangle in (b). The green, dashed line indicates the interface between GaAs and CIGS. The gradient in the CL intensity distribution perpendicular to the GaAs substrate can be attributed to higher [Ga] and thus higher bandgap energy close to the interface with GaAs. d) CL spectral linescan extracted along the black arrow in (c).

(enriched) in the lower left corner. As much as the Cu is enriched or depleted in the regions extending across several nm away from the dislocation cores, In was found to be depleted or enriched in these regions. Slight Se depletion was also detected in the Cu-enriched (In-depleted) region. This kind of redistribution has been found for various complete and partial dislocations in CIGS using STEM in combination with EELS[20,21] and using atom-probe tomography.[5,22] Always, Cu enrichment (depletion) and In as well as slight Se depletion (enrichment) were detected, with no detectable change in the Ga distributions, which indicates again (as for grain boundaries) at least a partial charge compensation involving the corresponding charged point defects Cu_{In}^{2-} (In_{Cu}^{2+}) and V_{Se}^{2+} (Se^{2-} on interstitial sites), including also O_{Se}. The depicted elemental redistribution is similar to the atomic reconstruction at grain boundaries in CIGS thin films,[2] only that the corresponding regions for dislocations are much wider (few nm) than at grain boundaries (<1 nm[25]).

Moreover, it was shown by Simsek Sanli et al.[21] that the spatial extensions of the regions with compositional changes around the dislocation cores agree well with the extensions of the strain fields around the dislocations. Thus, the pronounced Cu enrichment (depletion) as well as In/Se depletion (enrichment) can be regarded as a mechanism to relax the crystal lattice around the dislocation core. Consequently, this relaxation also affects the density of states, which is assumed to shift defects states closer to the band edges (similar to findings at CIGS grain boundaries with dislocation cores[23]), overall reducing nonradiative Shockley–Read–Hall recombination. We face a different scenario at (randomly oriented) grain boundaries, where strain accumulates[24] and where despite the atomic reconstruction of grain-boundary planes[25,26] considerable recombination velocities of several 100 cm s^{-1} even for high-efficiency devices are measured.[3] Nevertheless, CIGS solar cells with very high conversion efficiencies can be obtained by increasing the average grain sizes,
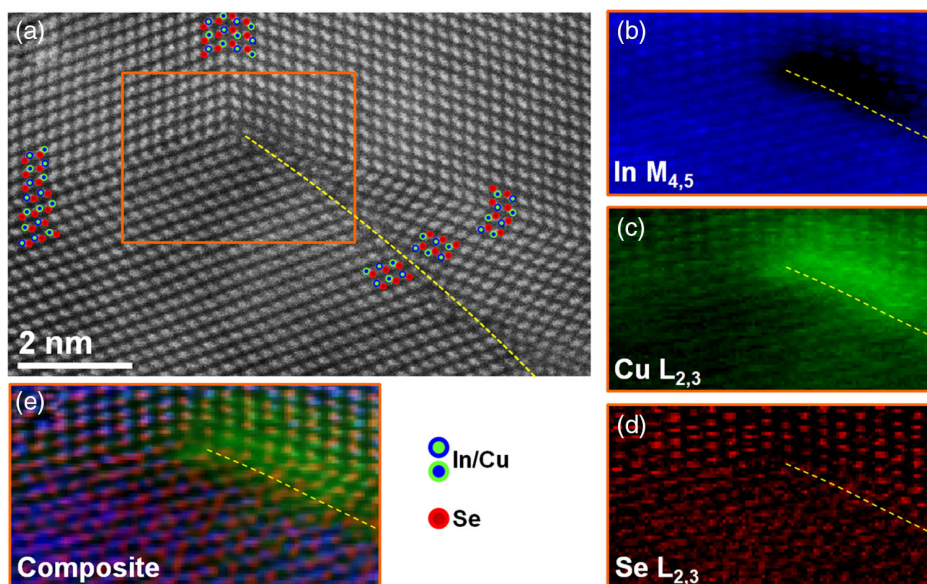
Figure 2. a) STEM HAADF image at a junction of three twin boundaries and a grain boundary in a CuInSe$_2$ thin film. b–d) Corresponding elemental distribution maps extracted from the electron energy-loss spectrum image, showing the integrated In–M$_{4,5}$, Cu–L$_{2,3}$, and Se–L$_{2,3}$ intensities. e) Composite image, a color-coded combination of Cu, In, and Se distribution maps, superimposed on a simultaneously acquired HAADF image. The grain boundary in (a) is composed of dislocation cores (along the yellow line). Strong Cu enrichment around the dislocation cores is accompanied by In and (slight) Se depletion at the identical atomic positions.

because dislocations—that might have higher densities in larger grains—do not exhibit effective centers of enhanced recombination.

5. Conclusions

This work provides direct evidence for an optoelectronic inactivity of dislocations in CIGS thin films, which is a unique behavior for a semiconductor material. We explain this extraordinary inactivity by the compositional flexibility of the CIGS lattice, providing the means for a strain-driven, elemental redistribution around dislocation cores, which relaxes the lattice and thus probably shifts defect states toward the band edges, leading to a similar nonradiative recombination behavior at line defects as in the CIGS bulk.

Conflict of Interest

The authors declare no conflict of interest.

Data Availability Statement

The data that support the findings of this study are available from the corresponding author upon reasonable request.

[1] M. Nakamura, K. Yamaguchi, Y. Kimoto, Y. Yasaki, T. Kato, T. H. Sugimoto, *IEEE J. Photovoltaics* **2019**, *9*, 1863.

[2] D. Abou-Ras, S. S. Schmidt, N. Schäfer, J. Kavalakkatt, T. Rissom, T. Unold, R. Mainz, A. Weber, T. Kirchartz, E. Simsek Sanli, P. A. van Aken, Q. M. Ramasse, H.-J. Kleebe, D. Azulay, I. Balberg, O. Millo, O. Cojocaru-Mirédin, D. Barragan-Yani, K. Albe, J. Haarstrich, C. Ronning, *Phys. Status Solidi RRL* **2016**, *10*, 363.

[3] M. Krause, A. Nikolaeva, M. Maiberg, P. Jackson, D. Hariskos, W. Witte, J. A. Márquez, S. Levcenko, T. Unold, R. Scheer, D. Abou-Ras, *Nat. Commun.* **2020**, *11*, 4189.

[4] J. Dietrich, D. Abou-Ras, T. Rissom, T. Unold, H.-W. Schock, C. Boit, *IEEE J. Photovoltaics* **2012**, *2*, 364.

[5] J. Dietrich, D. Abou-Ras, S. S. Schmidt, T. Rissom, T. Unold, O. Cojocaru-Mirédin, T. Niermann, M. Lehmann, C. T. Koch, C. Boit, *J. Appl. Phys.* **2014**, *115*, 103507.

[6] J. Dietrich, *Doctoral Thesis*, TU Berlin, Germany **2013**.

[7] A. M. Gabor, J. R. Tuttle, D. S. Albin, M. A. Contreras, R. Noufi, *Appl. Phys. Lett.* **1994**, *65*, 198.

[8] H. Stange, S. Brunken, D. Greiner, M. D. Heinemann, D. A. Barragan Yani, L. A. Wägele, C. Li, E. Simsek Sanli, M. Kahnt, S. S. Schmidt, J.-P. Bäcker, C. A. Kaufmann, M. Klaus, R. Scheer, C. Genzel, R. Mainz, *J. Appl. Phys.* **2019**, *125*, 035303.

[9] Y. Wang, Y. E. Suyolcu, U. Salzberger, K. Hahn, V. Srot, W. Sigle, P. A. van Aken, *Microscopy* **2018**, *67*, i114.

[10] S. Zaefferer, N. N. Elhami, *Acta Mater.* **2014**, *75*, 20.

[11] M. Müller, D. Abou-Ras, T. Rissom, F. Bertram, J. Christen, *J. Appl. Phys.* **2014**, *115*, 023514.

[12] A. Nikolaeva, M. Krause, N. Schäfer, W. Witte, D. Hariskos, T. Kodalle, C. A. Kaufmann, N. Barreau, D. Abou-Ras, *Prog. Photovoltaics: Res. Appl.* **2020**, *28*, 919.

[13] J. Kavalakkatt, D. Abou-Ras, J. Haarstrich, C. Ronning, M. Nichterwitz, R. Caballero, T. Rissom, T. Unold, R. Scheer, H. W. Schock, *J. Appl. Phys.* **2014**, *115*, 014504.

[14] D. Abou-Ras, N. Schäfer, T. Rissom, M. N. Kelly, J. Haarstrich, C. Ronning, G. S. Rohrer, A. D. Rollett, *Acta Mater.* **2016**, *118*, 244.

[15] J. Marek, R. Geiss, L. M. Glassman, M. P. Scott, *J. Electrochem. Soc.* **1985**, *132*, 1502.

[16] H. S. Leipner, J. Schreiber, H. Uniewski, S. Hildebrandt, *Scanning Microsc.* **1998**, *12*, 149.

[17] C. M. Parish, P. E. Russell, *Adv. Imaging Electron Phys.* **2007**, *147*, 1.

[18] M. Albrecht, J. L. Weyher, B. Lucznik, I. Grzegory, S. Porowski, *Appl. Phys. Lett.* **2008**, *92*, 231909.

[19] T. Sekiguchi, J. Chen, *Defects and Impurities in Silicon Materials*, Springer, Tokyo, Japan **2015**, pp. 343–373.

[20] E. Simsek Sanli, Q. M. Ramasse, W. Sigle, D. Abou-Ras, R. Mainz, A. Weber, H.-J. Kleebe, P. A. van Aken, *J. Appl. Phys.* **2016**, *120*, 205301.

[21] E. Simsek Sanli, D. Barragan-Yani, Q. M. Ramasse, R. Mainz, D. Abou-Ras, A. Weber, H.-J. Kleebe, P. van Aken, K. Albe, *Phys. Rev. B* **2017**, *95*, 195209.

[22] O. Cojocaru-Mirédin, T. Schwarz, D. Abou-Ras, *Scr. Mater.* **2018**, *148*, 106.

[23] Y. Yan, W. J. Yin, Y. Wu, T. Shi, N. R. Paudel, C. Li, J. Poplawsky, Z. Wang, J. Moseley, H. Guthrey, H. Moutinho, S. J. Pennycook, M. M. Al-Jassim, *J. Appl. Phys.* **2015**, *117*, 112807.

[24] E. Vasco, C. Polop, *Phys. Rev. Lett.* **2017**, *119*, 256102.

[25] D. Abou-Ras, B. Schaffer, M. Schaffer, S. Schmidt, R. Caballero, T. Unold, *Phys. Rev. Lett.* **2012**, *108*, 075502.

[26] D. Abou-Ras, S. Schmidt, R. Caballero, T. Unold, H.-W. Schock, C. Koch, B. Schaffer, M. Schaffer, P. Choi, O. Cojocaru-Mirédin, *Adv. Eng. Mater.* **2012**, *2*, 992.

2100042 (5 of 5)